*SAE TECHNICAL PAPER SERIES*

**941165**

# Results of a Rocket-Based Combined-Cycle SSTO Design Using Parametric MDO Methods

**John R. Olds**
North Carolina State University

**Aerospace Atlantic Conference and Exposition**
**Dayton, Ohio**
**April 18-22, 1994**

**400 COMMONWEALTH DRIVE, WARRENDALE, PA 15096-001 U.S.A. Tel:(412) 766-4841 Fax: (412) 776-5760**

# Results of a Rocket-Based Combined-Cycle SSTO Design Using Parametric MDO Methods

Dr. John R. Olds*
N. C. State University, Raleigh, NC

## ABSTRACT

This paper reports the results of the second phase of a research project to characterize and optimize the design of an advanced launch vehicle for human access to low earth orbit. The vehicle makes use of rocket-based combined-cycle (RBCC) propulsion — a concept combining operating modes of an ejector, ramjet, scramjet, and rocket in a single engine. This research builds on previous work focused on advanced multiple mode propulsion concepts and advanced conical acceleration-class single-stage-to-orbit (SSTO) launch vehicles.

Three systems level design variables of interest were optimized using multidisciplinary design optimization (MDO) techniques. Specifically, Taguchi's method of robust design was used to identify a combination of variables that minimize the vehicle sensitivity to unpredictable changes in engine weights and performance. In addition, a second-order response surface method (RSM) was used to approximate the design space and predict the minimum dry weight vehicle.

The optimized vehicle results (weights, dimensions, performance) are favorably compared with other SSTO designs including rocket and airbreathing concepts.

## NOMENCLATURE

| | |
|---|---|
| ACC | advanced carbon-carbon |
| Al-Li | aluminum-lithium |
| ANOM | analysis of the mean |
| APAS | aerodynamic preliminary analysis system |
| ATR | air-turborocket |
| $C_t$ | thrust coefficient |
| CCD | central composite design |
| $g_c$ | gravity constant (32.2 ft/s$^2$) |
| HABP | hypersonic arbitrary body program |
| $I^*$ | rocket equation effective specific impulse |
| Isp | specific impulse |
| IOC | initial operating capability |
| LH2 | liquid hydrogen |
| LOX | liquid oxygen |
| MDO | multidisciplinary design optimization |
| MER | mass estimating relationship |
| MR | mass ratio (lift-off weight/insertion weight) |
| NASP | national aerospace plane |
| OMS | orbital maneuvering system |
| PEEK | polyether-ether ketone |
| POST | program to optimize simulated trajectories |
| RBCC | rocket-based combined-cycle |
| RCS | reaction control system |
| RSM | response surface methods |
| S/N | signal-to-noise ratio |
| SSME | space shuttle main engine |
| SSTO | single-stage-to-orbit |
| $Ti_X$-Al | titanium-aluminide |
| TPS | thermal protection system |
| $T/W_o$ | lift-off thrust-to-weight ratio |
| UDP | unified distributed panel program |
| VMR | variable mixture ratio engine |
| $\Delta V$ | velocity change |
| $\phi$ | equivalence ratio |
| $\theta$ | cowl wrap angle |

## INTRODUCTION

NASA and the U.S. Department of Defense have for many years studied advanced launch vehicle concepts for transporting crew and cargo to and from low earth orbit. A variety of candidate concepts have

---

* - visiting assistant professor, mechanical and aerospace engineering dept. member SAE.

been considered including two-stage and single-stage concepts, partially and fully reusable concepts, and vehicles powered by rocket and airbreathing propulsion systems. Currently, designers believe single-stage, fully reusable launch vehicles may become feasible within the next decade and a half with moderate advances in technology.

Airbreathing SSTO concepts have been advocated as strong options due to their low overall gross weights, high average Isp's, plentiful abort options, mission flexibility (including hypersonic cruise), and potential for aircraft-like operations. The U.S. National Aerospace Plane (NASP) is such an option [1,2].

Rocket powered vehicle advocates claim lower dry (empty) weights, high engine thrust-to-weight ratios, fewer propulsion/airframe complexities, and reduced technology requirements. Several rocket SSTO vehicles are candidates including winged vehicles powered by either SSME-derivative engines [3] or dual-fuel concepts based on derivatives of the Russian RD-701 engine [4]. Non-winged concepts such as the Delta Clipper [5,6] are also being examined.

Multi-cycle and combined-cycle propulsion systems have been studied as ways to combine the best characteristics of airbreathing and rocket launch vehicles and to strike a balance between low gross weights and low dry weights (figure 1). Multi-cycle propulsion concepts include separate systems for each operating mode (e.g. a turbojet system *and* a rocket system). These systems may be operated separately or in parallel in order to maximize the performance of the overall vehicle. Combined-cycle propulsion systems integrate various operating modes into a single set of hardware components to minimize redundant systems and reduce propulsion system weight. Air liquefaction cycles and the rocket-based combined-cycles (RBCC) [7,8,9,10] are candidates from the latter set.

This paper reports the results of the second phase of a two phased study to optimize the design of a conical SSTO launch vehicle with RBCC propulsion. The study goal is to minimize vehicle dry weight (dry weight is considered a better indicator of vehicle cost than propellant dominated gross weight). The first phase results were reported in reference 11. Several

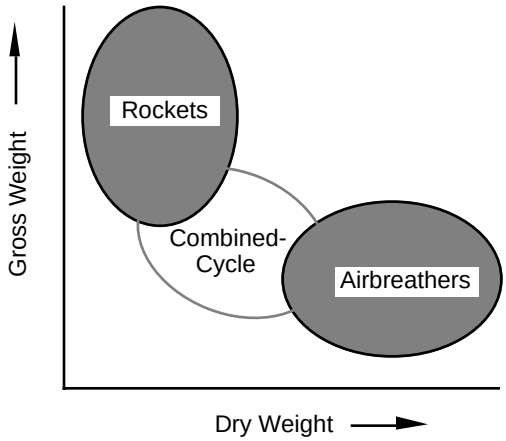


Figure 1 - Potential for Combined-Cycle Propulsion

systems level variables were established in phase 1. The present work establishes the remaining variables and makes comparisons with alternate airbreathing and rocket SSTO designs.

The RBCC SSTO design consists of many tightly coupled disciplinary analyses including performance, aerodynamics, aeroheating, propulsion, and weight estimation. Advanced conceptual-level computer programs were used to perform much of the analysis. In order to capture all of the complexities of the multivariable design, two techniques from the field of multidisciplinary design optimization (MDO) were employed — Taguchi's method of robust design and second-order response surface methods.

## VEHICLE DESCRIPTION

### Mission and Guidelines

For the purpose of this research, the candidate RBCC SSTO was sized to deliver a 10,000 lb (4,536 kg) payload to a polar parking orbit of 100 Nmi. x 100 Nmi. x 90° (185 km x 185 km x 90°). A fictitious facility at Vandenberg Air Force Base, California was assumed as the launch site. The vehicle payload bay volume was set to 5,300 $ft^3$ (150 $m^3$). When sized for the polar reference mission, the same vehicle will be capable of delivering slightly over 20,000 lbs (9,072 kg) to a 100 Nmi. x 100 Nmi. x 28.5° orbit from a launch site at Kennedy Space Center, Florida. The polar mission is similar to an early NASP design

reference mission and was chosen to allow easy comparison with several alternate vehicle concepts.

While recent design emphasis has focused on design for operations — larger margins, additional abort options, lower operating costs, and lower system complexities, the design philosophy employed for the present study is more closely related to design for performance. Again, this philosophy is consistent with that used for the rocket and airbreathing vehicles provided for comparison.

In addition to circularization and deorbit ΔV's, an on-orbit ΔV of 75 fps (25.6 m/s) is included in the vehicle OMS system. Provisions are included for a crew of 2 and a mission duration of 48 hours (typical for payload delivery and return missions). A weight margin of 10% was used for all dry weight components.

**Vehicle Configuration**

Previous research on airbreathing launch vehicles [1,12] and specifically research on rocket-based combined-cycle SSTO's [9,13,14] has identified potential advantages of a conical vehicle configuration. Specifically, a conical configuration offers well behaved forebody compression, high engine capture areas, and increased structural tank efficiencies. In some cases, circular cross section tanks may be appreciably lighter than non-circular cross section tanks of similar volume [15]. The basic vehicle configuration used for this research is shown in figure 2. The vehicle is fully reusable.

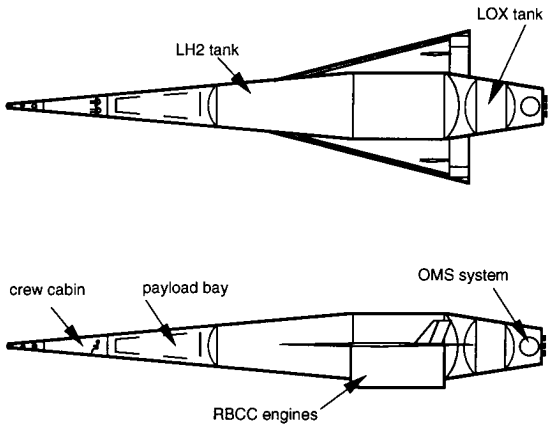


Figure 2 - RBCC SSTO Configuration

The vehicle consists of a large conical forebody enclosing the crew cabin, payload bay, and an integral LH2 tank. The cone half angle was set at 5° based on phase 1 results [11]. The engine cowl is wrapped around the cylindrical section of the LH2 tank. The length of the cylindrical section is determined by inlet geometry and the cowl wrap angle is an optimization variable. A 180° cowl wrap angle is shown in figure 2. The non-integral LOX tank and the rear cryogenic OMS propellant tanks are located in the vehicle tailcone. Small RCS tanks are also located in the vehicle nose. The delta wing (based on previous work) is 4% thick, has an aspect ratio of 1, and has a leading edge sweep angle of 76°[12,16]. The main landing gear is stored in unused regions of the cowl on the bottom of the vehicle. The nose gear is deployed from an area below the payload bay. The payload is loaded and deployed through a set of hinged doors on top of the payload bay.

**Technologies and Materials**

The RBCC SSTO is designed to have an initial operating capability (IOC) between the years 2005 and 2010. Many advanced technologies and materials are used throughout the design as shown in table 1.

Table 1 - Advanced Technologies

| | |
|---|---|
| Propellant Tanks | • Graphite/PEEK filament wound LH2 tank<br>• Al-Li LOX tank<br>• composite overwrapped OMS tanks |
| Structures & TPS | • $Ti_xAl$ wing, tailcone, cowl, nosecone<br>• advanced metallic & ACC TPS<br>• active LH2 cooling in high temp areas |
| Propulsion | • advanced RBCC engine<br>• cryogenic OMS & RCS systems |
| Subsystems | • electromechanical actuators<br>• advanced landing systems<br>• lightweight avionics and power systems |

Single-stage-to-orbit vehicles are extremely sensitive to weight growth. Without the weight saving advantages of these technologies, the present RBCC SSTO design would quickly become infeasible. Many advanced technologies are currently being developed under the NASP technology program.

**RBCC Engine**

The vehicle is powered by a rocket-based combined-cycle (RBCC) propulsion system. The RBCC engine as been the subject of several research efforts — in the mid-1960's [17] and more recently [8,9,10,11,13,14]. Reference 17 presents the results of Marquardt's broad examination of several RBCC options including engines with and without supercharging fans, engines with and without liquid air cycles, and engines with and without scramjet capability. Two engines were identified as the most viable candidates for application to future launch vehicles. Both selected engines (given the designations #10 and #12) were capable of scramjet operation, but neither employed a liquid air cycle. Engine #12 had a supercharging fan in the inlet to provide additional performance at low speeds. Engine #10 had no fan, but was lighter weight. Weight statements and performance information for these engines are available in reference 17.

In 1988, Foster [14] reevaluated and updated the RBCC engine data and compared several *conical* SSTO launch vehicles based on RBCC propulsion (figure 3). The work demonstrated the potential weight and performance advantages of the concept. In addition, Foster's work helped identify many of the key systems level variables used in the present study.

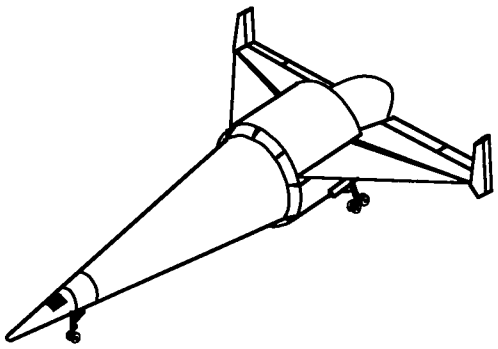

Figure 3 - RBCC SSTO from Reference 14

One of the preferred engines from Foster's work is shown in figure 4. It is based on engines from reference 17. A slightly modified and more parameterized version of this engine concept was used for the present research.

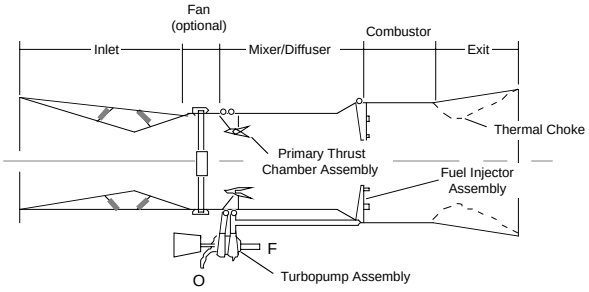


Figure 4 - RBCC Engine Layout

The RBCC engine is an air-augmented LOX/LH2 engine capable of operation in four distinct modes — ejector, ramjet, scramjet, and rocket. In ejector mode, the rocket primary serves as a "pump" to entrain additional atmospheric air through the inlet. The entrained air is mixed with the rocket primary exhaust and additional fuel and burned in an afterburner fashion. The rocket primary is turned off in ramjet and scramjet modes, and oxidizer is provided solely by atmospheric air. In rocket mode, the inlet can be closed off, and the engine operates as a high expansion ratio rocket.

## ANALYSIS METHODS

Several conceptual level computerized analysis programs were used to accomplish this design. These tools were typically associated with distinct disciplines, and the level of analysis detail obtained was commensurate with conceptual aerospace vehicle design. In some cases, highly detailed analysis (e.g. full Navier-Stokes solutions for aerodynamic coefficients) was sacrificed in favor of reduced analysis time and the ability to quickly consider several configurations.

**Trajectory/Performance**

Ascent trajectory analysis for the RBCC SSTO was performed using 3D POST (Program to Optimize Simulated Trajectories) [18]. POST integrates the equations of motion for a generalized point mass vehicle from lift-off to orbital insertion through various user defined guidance phases. The program automatically adjusts trajectory parameters in order to optimize the ascent (minimize ascent propellant in this case) while satisfying all constraints.

The vehicle ascent was simulated using a vertical lift-off from Vandenberg AFB, ejector mode engine operation to Mach 3, followed by ramjet/scramjet mode engine operation along a constant 2000 psf (95,760 Pa) dynamic pressure boundary to the prescribed airbreathing to rocket mode transition Mach number ($M_{tr}$). The engine was operated in rocket mode for acceleration to an optimum intermediate parking orbit and OMS engines were used for the final insertion into a 100 Nmi. (185 km) circular polar orbit. For this study, the ascent was flown untrimmed and reentry trajectories were not considered.

POST requires aerodynamic tables, engine performance tables, and vehicle weights and sizes as inputs. POST outputs include minimum propellant required (in the form of a mass ratio, MR), hydrogen fuel/total propellant ratio (changes depending on airbreathing portion of the trajectory), altitude, velocity, and angle-of-attack vs. time histories, and an indication of the maximum wing loading along the trajectory.

**Aerodynamics**

Aerodynamic analysis was performed using APAS (Aerodynamic Preliminary Analysis System) [19] for selected Mach numbers and angles of attack throughout the speed regime (0 to Mach 25). APAS consists of two modules — UDP for subsonic/supersonic analysis and HABP for hypersonic analysis. UDP (Unified Distributed Panel program) uses a panel method with linearly varying sources and vortices. Slender body theory is used to analyze vehicle fuselages. Viscous and wave drag terms are added empirically. HABP (Hypersonic Arbitrary Body Program) uses appropriate impact pressure methods (e.g. modified Newtonian, tangent cone) for different sections of the vehicle. Empirical base drag calculations were included for both powered and unpowered analyses.

For powered flight/ascent, the tailcone of the RBCC SSTO was treated as part of the engine nozzle in order to be consistent with available engine data [16]. The forebody, wings, and exterior cowl were treated as aerodynamic surfaces. For unpowered flight and landing, the entire vehicle was treated aerodynamically. The delta wing was scaled to provide a landing speed of less than 200 knots (102.9 m/s) at an angle of attack of 15° based on the current landing weight. The vehicle wing was located longitudinally (fore to aft) in order to provide static stability (with flaps deflected) at typical hypersonic entry and landing conditions.

APAS requires vehicle geometry, landing weight, and c.g. location as inputs. Outputs produced by APAS include aerodynamic coefficients ($C_l$ and $C_d$ tables vs. Mach number and angle of attack), required wing planform area, landing configuration wing loading, and longitudinal wing position.

**Aeroheating**

Aerodynamic heating analysis was performed using Miniver [20]. Miniver uses appropriate empirical heating methods (e.g. Eckert reference enthalpy for flat plates, Cato/Johnson for swept cylinders, etc.) to estimate heat load and heating rates for various locations on the vehicle body during ascent. For each RBCC SSTO configuration and ascent trajectory, radiation equilibrium temperatures were determined along the forebody windward and leeward centerlines, along the cowl windward and leeward centerlines, and along a representative wing cross section for both windward and leeward sides. The majority of the thermal protection system (TPS) on the RBCC SSTO is assumed to be of a passive, radiative type — either advanced carbon-carbon (ACC), Inconel tiles, or Titanium tiles. Although the total heat load for airbreathing vehicles is high, the weight of the TPS is primarily determined by material characteristics required to withstand the surface temperature. Therefore, the maximum surface temperatures for the six reference lines above were used to select TPS type for various acreage areas of the vehicle. For the forebody and cowl, the lower 120° of surface arc was associated with the windward centerline temperature and the upper 240° of surface arc was associated with the leeward surface temperature. ACC was used for surface temperatures below 3000°F (1922°K), Inconel was used for temperatures below 1800°F (1255°K), and Titanium was used for temperatures below 1200°F (922°K). In the case of the wing and cowl, the primary structure of the RBCC SSTO, Titanium-Aluminide Beta 21S, was capable of withstanding surface temperatures up to 1500° F (1089°K) without TPS.

Active cooling methods consisting of circulating liquid hydrogen (LH2) through cooling panels and passages and heat conduction methods like heat pipes were used in high temperatures areas such as the vehicle nose, the wing leading edges, the cowl lip, and the area immediately aft of the internal engine nozzle. These areas will be exposed to temperatures several times higher than ACC is capable of withstanding.

Miniver requires vehicle geometry and ascent trajectory information (altitude, velocity, and angle-of-attack vs. time) as inputs. Miniver provides maximum radiation equilibrium temperatures for various body locations as outputs.

**Propulsion**

The RBCC engine is capable of operating in four distinct modes. Complete engine performance information (thrust and Isp) was created for each engine/vehicle configuration. The engine inlet/cowl geometry was largely determined by the maximum airbreathing Mach number ($M_{tr}$). The maximum inlet height was determined by shock-on-lip conditions at $M_{tr}$ for the current forebody size and length. Higher $M_{tr}$'s mandate smaller inlet heights. In no case was the inlet height allowed to exceed 4.5 ft (1.38 m). Inlet length was scaled with inlet height and $M_{tr}$. Larger $M_{tr}$'s require longer inlet lengths. Engines were considered modular. Each engine occupied about 20° of vehicle circumference. For example, there were 18 separate engines for vehicles with 360° of cowl wrap. Cowl wrap angle and inlet height combined to prescribe inlet capture area (the annular area). Diffuser/mixer, combustor, and internal nozzle lengths were determined based on capture area. Reference 21 contains additional detail on engine scaling.

For ejector mode operation up to Mach 3, engine thrust and Isp tables vs. altitude and Mach number were determined using a quasi-1D compressible flow model of each of the components in the engine flow path. The technique and component efficiencies are described in reference 17. In ejector mode, the thrust of the overall engine is largely governed by the mass flow rate through the rocket primary (rather than by the entrained air through the inlet). For a given capture area, the size of the rocket primary was increased or decreased in order to obtain the required vehicle thrust-to-weight ratio ($T/W_o$) at lift-off. Therefore, the sea-level static ratio of rocket primary mass flow to inlet air mass flow was not constant across all designs.

Between Mach 3 and $M_{tr}$, the engine was operated in ramjet and then scramjet mode. Existing data on ramjet/scramjet engine performance for a winged-cone [16] was used to *approximate* RBCC performance in these modes. The existing data was tabulated as $C_tA_{ref}$ and Isp vs. Mach number, altitude, and equivalence ratio ($\phi$). $C_t$ is the thrust coefficient where:

$$thrust = (C_t A_{ref}) \frac{A_c}{A_{ref}} q \qquad (1)$$

thrust = thrust in lbs (cowl-to-tail)
q = freestream dynamic pressure in psf ($\rho V^2/2$)
$A_c$ = annular engine capture area in $ft^2$
$A_{ref}$ = reference area in ref. 16 = 207 $ft^2$

The equivalence ratio ($\phi$) is the ratio of mass flow rate of hydrogen fuel to the mass flow rate of hydrogen required for stoichiometric combustion. $\phi$ is similar to a throttling parameter for thrust, but increasing $\phi$'s have a negative impact on Isp. $\phi$ was allowed to vary during ascent, but in order to provide adequate engine cooling at high Mach numbers, additional hydrogen circulation is required. Therefore, $\phi$ was not allowed to fall below a line formed by $\phi$=1 at Mach 12 and $\phi$=2.5 at Mach 18. The vehicle tailcone is considered part of the engine nozzle in reference 16 (i.e. all values are "cowl-to-tail").

In rocket mode, the RBCC engine is treated as a throttleable, high expansion ratio rocket engine capable of a vacuum Isp of 470 sec [14]. Rocket mode vacuum thrust was determined by multiplying Isp by the maximum ejector weight flow rate and a variable throttle setting. An equivalent exit area was determined based on vehicle tailcone geometry.

The ratio of hydrogen fuel to total ascent propellant consumed during ascent depends on the trajectory and the amount of time spent in each engine mode. For ejector operation, the ejector component operates at stoichiometric mixture ratio (LOX/LH2 =

8), but additional hydrogen is used in order to burn the oxygen in the entrained air at stoichiometric ratios. Therefore, the ejector mode LOX/LH2 mixture ratio depends on flight conditions, but is always less than 8. In ramjet and scramjet modes, all propellant consumed is hydrogen since oxygen is provided by the atmosphere. In rocket mode, the engine operates at an LOX/LH2 mixture ratio of 6. The ratio of hydrogen fuel to total ascent propellant is used to determine the relative sizes of the LH2 and LOX tanks.

The engine analysis requires initial thrust requirements (to match a given $T/W_O$), transition Mach number, body circumference, and forebody length as inputs. Engine analysis outputs include ejector mode performance tables, engine length, engine capture area, inlet height, engine weight, and ejector component maximum mass flow rate.

**Weights and Sizing**

In order to match the required mass ratio (MR) from ascent analysis, the main hydrogen tank was sized up or down while maintaining a constant forebody cone half-angle of 5°. All other tanks and geometry were also resized accordingly (e.g LOX tank volume is related to LH2 tank volume, tailcone size is related to LH2 tank diameter and aft cone angle). A larger hydrogen tank will provide a larger MR. During the resizing process, some geometry remained fixed. For example, the payload bay size and the crew cabin size did not change when the LH2 tank was resized. Geometric resizing was accomplished using highly interdependent geometry equations on a computerized spreadsheet. LH2 tank maximum diameter was used as the independent variable. All other dimensions and geometry were calculated from LH2 tank diameter.

For each trial LH2 tank diameter, a mass ratio was determined by calculating the lift-off weight and the insertion weight. The calculation of the weight of a vehicle configuration is the most critical part of conceptual vehicle design. In particular, single-stage-to-orbit launch vehicles are highly sensitive to small changes in estimated weight. The system, component, and subsystem weights for the RBCC SSTO were determined using relatively detailed mass estimating relationships (MER's). MER's relate the weight of a component to vehicle parameters such as size, technology level, or loads. For example, wing weight is a function of size, construction method, geometry, and load. OMS propellant requirements are a function of orbital vehicle weight, engine performance, propellant mixture ratio, and orbital velocity change requirements. Most MER's are derived from regression analysis of historical data and are extrapolated to account for advanced technology. A complete list of MER's used for this vehicle is available in reference 21. In most cases, the MER's are derived from equations used for similar advanced SSTO vehicles including the airbreathing vehicle in reference 1 and the $Ti_X$-Al rocket vehicle in reference 22. The RBCC engine weight is highly dependent on engine geometry and vehicle geometry. Specific weight values from engine point designs in reference 14 and reference 17 were parameterized as noted in reference 21 for both airbreathing and rocket components. These parameterized engine MER's were used to predict engine weight for each vehicle design.

The weight and sizing analyses are very tightly coupled. Vehicle weights were calculated on the same spreadsheet as the vehicle geometry. Changes in LH2 tank diameter initiated an iterative solution for new sizes, weights, and MR. LH2 tank diameter was adjusted until the vehicle MR matched the required MR from ascent analysis. The weights and sizing spreadsheet requires TPS types for various acerage areas, LH2 propellant/total propellant ratio, required MR, peak wing loads, landing weight/wing reference area, engine dimensions, engine weights, and orbital circularization $\Delta V$ as inputs. Spreadsheet outputs include vehicle geometry, lift-off weight, landing weight, c.g. location, and lift-off thrust requirements.

## DESIGN PROCESS

Based on the previous research of reference 14, eight systems-level design variables were originally selected for study in this project. As reported in reference 11, five variables were adequately determined in phase 1 (table 2). (Unfortunately the RBCC SSTO weights reported in reference 11 are not directly comparable to those reported in this paper. Phase 2 work was performed on a vehicle with a larger payload bay, increased cowl strut weights, and the elimination of a redundant

margin on engine weights. The phase 2 results are about 6% heavier in terms of dry weight than phase 1 results, but phase 1 design variable results are still considered valid). The goal of phase 2 of this project was to determine the optimum values for the remaining three variables (table 3 and figure 5). The objective was to minimize vehicle dry weight.

Table 2 - Phase 1 Design Variable Results

| Variable | Phase 1 Results |
|---|---|
| max. dynamic pressure | 2000 psf |
| cone half angle | 5° |
| stag. point heat rate limit | 350 BTU/sq-ft-sec |
| supercharged engine? | no (engine 10) |
| take-off mode | vertical |

Table 3 - Phase 2 Design Variables

| Variable | Low Range | High Range |
|---|---|---|
| vehicle liftoff $T/W_O$ | 1.2 | 1.4 |
| cowl wrap angle ($\theta$) | 180° | 360° |
| scramjet to rocket transition Mach number | 12 | 15 |

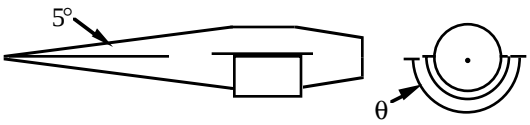


Figure 5 - Cowl Wrap Angle ($\theta$)

**Optimization Techniques**

As reported in reference 11, Taguchi methods were used to predict the near optimum settings of the design variables for phase 1. Taguchi methods are related to statistical-based design of experiments methods. In both methods, a fixed number of experimental points in the design space is strategically selected for analysis. The near-optimum values for the design variables are then predicted (interpolated) from the experimental results using an additive model [23,24,25]. Taguchi methods make use of orthogonal experimental arrays and are suitable for multidisciplinary problems with discrete variables [26]. Several successful aerospace design applications have been recently reported [27,28].

For phase 2 of this research, an optimization was performed using Taguchi's method of robust design [23]. Robust design allows designers to select variable settings that will yield a reduced sensitivity to uncontrollable, and potentially detrimental "noise" factors. Noise factors are assumed to be controllable for the purpose of a series of experiments (i.e. point designs), but are not controllable in the "real" world. Making use of orthogonal experimental arrays, Taguchi developed a technique based on signal-to-noise ratios (S/N) where each point design in an experimental array is subjected to several combinations of noise factors. For each of these point designs, an overall S/N is calculated as follows:

$$S/N = -10*\log_{10}\left(\frac{1}{4}\sum_{i=1}^{4} y_i^2\right) \qquad (1)$$

Similar to basic Taguchi methods, the S/N ratio is maximized using an analysis of the mean (ANOM) technique on each term in an additive model. A larger S/N represents a lower sensitivity to noises, and therefore a more robust design.

For the RBCC SSTO design, three factors were considered to be noises (table 4). In table 4, 0% represents no change from the nominal values used, +20% indicates a 20% increase (for weights), and -20% indicates a 20% drop in engine Isp at high Mach numbers. The objective of the robust design application was to select the values of the design variables (table 3) that will provide a low vehicle dry weight while minimizing the vehicle's sensitivity to engine weight growth (in the airbreathing components), engine Isp degradation, and vehicle fuselage structural weight growth. That is, the robust

Table 4 - Noise Variables for Robust Design

| Variable | Low Range | High Range |
|---|---|---|
| engine Isp degradation, $N_{isp}$ | -20% | 0% |
| engine weight growth, $N_{eng}$ | 0% | +20% |
| vehicle fuselage weight growth, $N_{fuse}$ | 0% | +20% |

vehicle's dry weight should not grow excessively if the nominal estimates for any of the noise variables changes by up to 20%. Additional detail is available in reference 21.

In an attempt to improve the accuracy of the optimum, a second-order response surface method (RSM) was also employed in phase 2 (made possible by the fact that there were only 3 continuous design variables). In response surface methods, a central composite design (CCD) experimental array is used to determine a set of point designs that can be used to fit a regression model of the form:

$$y = \beta_0 + \sum_{i=1}^{n} \beta_i x_i + \sum_{i=1}^{n} \sum_{j=i+1}^{n} \beta_k x_i x_j + \sum_{i=1}^{n} \beta_l x_i^2 \quad (2)$$

y = dry weight
$x_i$ = design variables
$\beta_i$ = equation constants

The second-order response surface can then be minimized using a non-linear optimizer. While RSM's actually optimize an *approximation* to the true design space (second-order model), rather than the actual design space, they represent an excellent balance between accuracy and design time. Techniques for constructing central composite designs are discussed in reference 29. A more detailed explanation of the use of CCD's and RSM's for this application is available in reference 21.

**Generation of Candidate Designs**

For each combination of design variables in an experimental array, a complete, converged solution for a candidate RBCC SSTO was generated. Each design required several passes through all of the disciplinary analysis tools. For a given $T/W_o$ at lift-off, cowl wrap angle, and $M_{tr}$, the analysis proceeded according to figure 6. Iteration for loop 1 was performed automatically on the weights and sizing spreadsheet. All variables converged to with a tolerance of <.001% after about 10-12 automatic iterations. Iteration loop 2 was a manual iteration between two complex spreadsheets. Exchanged variables generally converged to within a tolerance of <.01% in 3-4 iterations. Note that each iteration of loop 2 also required a separate execution of loop 1. Iteration loop 3 was a manual iteration between several separate disciplinary analysis tools. In each case, required information was manually exchanged between each tool. Loop 3 was repeated until MR converged to within 1% — typically 3-4 iterations. Each iteration of loop 3 required separate complete solutions for loop 2 and loop 1.

Since most of the design codes were separate, non-integrated computer tools, the process to produce a single, converged point design typically took 6-8 hours of real time. However, actual required CPU time was as much as two orders of magnitude lower. This design process could benefit tremendously from code integration (i.e. one code calling the next and automatically exchanging data). However code integration is time consuming and may suffer from inflexibility. The present "loosely coupled" arrangement is probably more typical of design

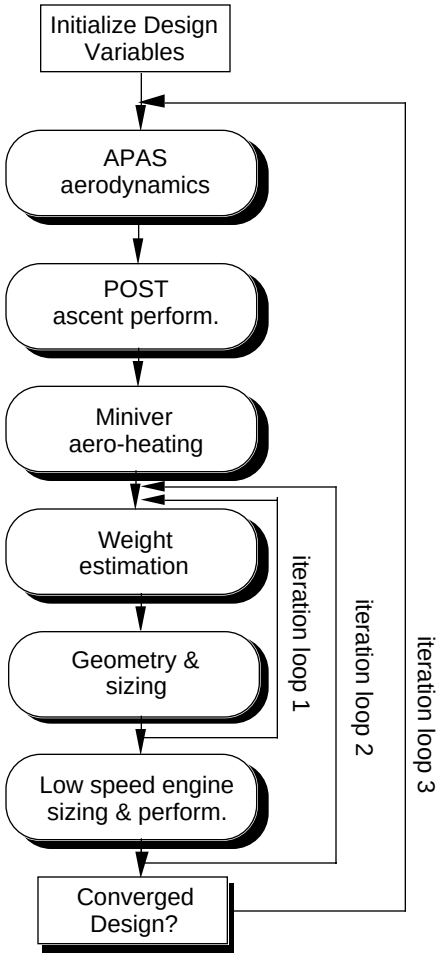


Figure 6 - Analysis Loops

Table 5 - Dry Weight Results (lbs) for $L_8$ by $L_4$ Robust Design Experiments

| $T/W_o$ | $M_{tr}$ | θ | 0% 0% 0% | 0% 20% 20% | -20% 0% 20% | -20% 20% 0% | $N_{isp}$ $N_{eng}$ $N_{fuse}$ | S/N |
|---|---|---|---|---|---|---|---|---|
| 1.2 | 12 | 180° | 92,498 | 118,623 | 119,865 | 109,261 | | -100.875 |
| 1.2 | 12 | 360° | 125,091 | 161,283 | 154,076 | 151,943 | | -103.448 |
| 1.2 | 15 | 180° | 92,121 | 123,229 | 131,979 | 117,139 | | -101.368 |
| 1.2 | 15 | 360° | 118,731 | 162,323 | 166,299 | 165,534 | | -103.780 |
| 1.4 | 12 | 180° | 92,871 | 120,909 | 122,145 | 110,463 | | -101.001 |
| 1.4 | 12 | 360° | 124,903 | 161,361 | 153,085 | 151,701 | | -103.428 |
| 1.4 | 15 | 180° | 91,685 | 124,938 | 135,532 | 118,943 | | -101.502 |
| 1.4 | 15 | 360° | 118,690 | 161,095 | 164,714 | 163,823 | | -103.711 |

Table 6 - S/N ANOM Averages for Robust Design

| | $T/W_o$ | $M_{tr}$ | θ | $T/W_o$ x $M_{tr}$ | $T/W_o$ x θ | $M_{tr}$ x θ |
|---|---|---|---|---|---|---|
| L | **-102.368** | **-102.188** | **-101.187** | -102.394 | -102.433 | -102.437 |
| H | -102.411 | -102.590 | -103.592 | **-102.384** | **-102.346** | **-102.342** |
| β's | -0.021 | -0.201 | -1.203 | 0.005 | 0.044 | 0.047 |

processes as they exist in most industry and government preliminary design organizations.

## RESULTS

### Robust Design

To capture all desired interaction effects using Taguchi's method of robust design, the three design variables (table 3) were placed in an $L_8$ orthogonal array and the three noise variables (table 4) were placed in an $L_4$ orthogonal array [21]. The two arrays were arranged as shown in table 5. Each row – column intersection in the $L_8$ by $L_4$ arrangement represents a point in the design space. 32 complete, converged point designs were generated and the dry weights (in lbs) were tabulated. Signal-to-noise ratios were calculated for each row using equation 1.

Experimental arrays with two variable levels ("settings") are only capable of fitting linear models. Therefore, we would expect the predicted maximum S/N to occur at one of the corners of the design space when each design variable is limited to "low" and "high" extremes as shown in table 3. That is, the predicted maximum S/N will be at a point represented by a combination of either the low or high bound on each design variable. Since there are only three design variables and eight ($2^3$) possible combinations, we should expect that one of the rows of the $L_8$ experimental array will correspond to the predicted maximum S/N.

By using Taguchi's orthogonal (i.e. balanced) experimental arrays, selection of the best design point is reduced to a very simple process. Rather than actually fitting the S/N data to a linear model, Taguchi recommends using an analysis of the mean (ANOM) table (table 6). Each design variable in the eight row experimental array has two settings — low and high. Since the array is balanced, there are 4 experiments at each of the two settings (for each variable). The average S/N values at each of the two settings are calculated and placed in the ANOM table [23]. The β's in table 6 correspond to the coefficient that each term would have in a linear regression model based on

normalized design variable values between -1 and +1. The β's are calculated as (H-L)/2.

Interaction effects (i.e. how one variable depends on another) are represented by "cross-terms". Cross terms are analogous to a product term between two design variables in a regression model. For example, for rows where $T/W_o$ is low (1.2) and $M_{tr}$ is low (12), the cross term $T/W_o$ x $M_{tr}$ is high. Interaction effects between variables are also balanced for each of their two settings, and the average S/N's are listed in table 6. The actual settings of the interaction terms depend on the settings of the design variables.

In this case, the overall S/N will be maximized if each design variable is set to the level that maximizes it's individual S/N average (keeping in mind that selection of main variable settings will affect the interaction settings). For the RBCC SSTO, selection of the **low** range for each of the three design variables will produce the largest S/N (table 7). This point corresponds to row #1 and a maximum S/N of -100.875. The magnitudes of the β's in table 6 give a relative indication of the influence of each term on the overall S/N. Note that the largest effect on S/N is due to cowl wrap angle, θ. A θ of 180° is strongly preferred. $M_{tr}$ is the second most significant effect (12 is best), while $T/W_o$ shows very little effect.

Table 7 - Robust Design Variable Levels

| | |
|---|---|
| $T/W_o$ | 1.2 |
| $M_{tr}$ | 12 |
| Cowl Wrap Angle, θ | 180° |

The objective of the robust design is to minimize the sensitivity to uncontrollable noise factors, while still providing a low dry weight. At the nominal noise variable settings (column 1 from table 5), the robust design variable settings produce a RBCC SSTO with a dry weight of 92,498 lbs (41,957 kg). However, the design variable combination in row #7 (changing $T/W_o$ to 1.4 and $M_{tr}$ to 15) would produce a *lower* vehicle dry weight of 91,685 lbs (41,588 kg). The advantage of the robust design is clearly evident, however, by scanning across row #1 and comparing the relative weight increases to those in row #7. If the engine performance is below current predictions, the engine weight grows, and/or the vehicle fuselage weight grows, then the robust vehicle design will be relatively less affected than the vehicle designed with settings corresponding to row #7. Therefore, it would be wise to sacrifice a small amount of dry weight at the nominal noise settings in order to gain the benefits of robustness.

As applied here, Taguchi's method of robust design is essentially a linearization of the design space in terms of S/N. The best settings for each design variable were necessarily at one end of their allowable range or the other. The *true* function for S/N could have a maximum somewhere inside the design space. Additional S/N benefit could probably be derived from relaxing the lower bounds on the design variables (particularly cowl wrap angle to a value less than 180°). However, the results presented here are very useful in characterizing the design space. For example, an earlier transition from airbreathing to rocket propulsion (i.e. a lower $M_{tr}$) is preferred if the designer is concerned about a possible degradation of engine $I_{sp}$ at high speeds. However, if engine performance meets or exceeds current predictions, a higher $M_{tr}$ (up to 15) will produce a lighter vehicle.

**Second-Order Response Surface**

In order to increase the accuracy of the optimization and to create a better model for "what-if" type analysis, an extra set of point designs was generated and added to the 32 experiments of table 5. Previous experiments were conducted at only two settings for each variable — thereby yielding only a linear model. The seven additional points (one center point and six "star" points) in table 8 allow the formation of a 39 row central composite design (CCD) experimental array and the use of a second-order response surface model [21].

The 32 point designs performed for the robust design do not allow two factor interaction terms between noise variables to be estimated. The seven runs added for the CCD allow estimation of second-order terms for the three main design variables, but not for the noise variables. Both of the omitted effects are assumed to be small in this example.

Table 8 - Additional Point Designs for CCD

| $T/W_o$ | $M_{tr}$ | $\theta$ | $N_{isp}$ | $N_{eng}$ | $N_{fuse}$ | Dry Weight (lbs) |
|---|---|---|---|---|---|---|
| 1.3 | 13.5 | 270° | -10% | +10% | +10% | 127,552 |
| 1.1 | 13.5 | 270° | -10% | +10% | +10% | 129,163 |
| 1.5 | 13.5 | 270° | -10% | +10% | +10% | 128,921 |
| 1.3 | 10.0 | 270° | -10% | +10% | +10% | 128,467 |
| 1.3 | 17.0 | 270° | -10% | +10% | +10% | 136,295 |
| 1.3 | 13.5 | 360° | -10% | +10% | +10% | 109,221 |
| 1.3 | 13.5 | 180° | -10% | +10% | +10% | 149,310 |

A least squares regression fit of the 39 experimental point designs yields the following second-order model for dry weight (in lbs):

$$\begin{aligned}
&\text{Dry Weight(lbs)} = \\
&126,668 + 159\left(\frac{\hat{T}}{W}\right) + 2,447\hat{M}_{tr} + 18,310\hat{\theta} \\
&-7,692\hat{N}_{isp} + 6,821\hat{N}_{eng} + 10,502\hat{N}_{fuse} \\
&-85\left(\frac{\hat{T}}{W} * \hat{M}_{tr}\right) - 584\left(\frac{\hat{T}}{W} * \hat{\theta}\right) - 55\left(\frac{\hat{T}}{W} * \hat{N}_{isp}\right) \\
&+29\left(\frac{\hat{T}}{W} * \hat{N}_{eng}\right) + 167\left(\frac{\hat{T}}{W} * \hat{N}_{fuse}\right) - 349(\hat{M}_{tr} * \hat{\theta}) \\
&-3,005(\hat{M}_{tr} * \hat{N}_{isp}) + 508(\hat{M}_{tr} * \hat{N}_{eng}) \\
&+963(\hat{M}_{tr} * \hat{N}_{fuse}) - 914(\hat{\theta} * \hat{N}_{isp}) \\
&+2,771(\hat{\theta} * \hat{N}_{eng}) - 263(\hat{\theta} * \hat{N}_{fuse}) + 657\left(\frac{\hat{T}}{W}\right)^2 \\
&+1,084(\hat{M}_{tr})^2 + 3,616(\hat{\theta})^2
\end{aligned}$$

Equation 3 - Second-Order Response Surface

In equation 3, the three design variables and three noise variables have been *normalized* so that a normalized value of -1 corresponds to the original variable low range and +1 corresponds to the original variable high range as given in tables 3 and 4 respectively. Therefore, the variables on the right hand side of equation 3 are dimensionless. The magnitudes of the equation coefficients indicate the relative impact that each term will have on vehicle dry weight as variables are moved from one end of their range to another. For example, the cowl wrap angle has the largest influence on vehicle dry weight, and the noise variables have a significant impact. As with the S/N analysis, $T/W_o$ has only a small influence on the design. Note the strong interaction between $M_{tr}$ and engine Isp ($N_{isp}$). As engine Isp degrades (normalized $N_{isp}$ becomes more negative), a lower (more negative) $M_{tr}$ is preferred.

Equation 3 can be minimized (subject to variable range limits). The point that minimizes dry weight is shown in table 9. As expected, the three noise variables are optimized to their nominal (baseline values). Recall that any perturbations to noises would have a negative impact on the vehicle. $\theta$ is limited (somewhat artificially) by the lower end of its allowable range. It is highly probable that additional dry weight savings could be realized with a cowl wrap angle of less than 180°. As discussed previously, a $M_{tr}$ near 15 tends to produce a lighter (but less robust) launch vehicle. The optimum $M_{tr}$ for dry weight is 14.6. Again, $T/W_o$ has only a small effect on the dry weight.

At the minimum conditions, the model predicts a dry weight of 89,660 lbs (40,670 kg). An actual experiment at that point produced a vehicle dry weight of 91,578 lbs (41,540 kg) — an acceptable difference of 2.1%. Recall that the previous lowest dry weight was 91,685 lbs (41,588 kg) at row #7, column #1 of the 32 experiment robust design array. The design variable values are very similar for the two points. For this case, the second-order model does not improve significantly on the linear model.

Table 9 - Minimum Dry Weight for Second-Order Response Surface

| | |
|---|---|
| $T/W_o$ | 1.27 |
| $M_{tr}$ | 14.6 |
| Cowl Wrap Angle, θ | 180° |
| $N_{isp}$ | 0% |
| $N_{eng}$ | 0% |
| $N_{fuse}$ | 0% |

In addition to providing an approximation of the minimum vehicle dry weight, equation 3 is very useful to the designer for quickly answering "what-if" questions without having to reevaluate an entire vehicle point design. For example, the impacts of engine Isp degradation or engine weight growth can easily be approximated.

**Final Vehicle Design**

Even though the second-order response surface method produced the lowest dry weight, the **robust** design variable settings were selected for the final design (table 7). The robust design is less sensitive to changes in the noise variables and only has a slight weight penalty at nominal noise values.

The final RBCC SSTO configuration is shown in figure 7. The vehicle dry weight is 92,498 lbs (41,957 kg) and the gross lift-off weight (fueled) is 506,575 lbs (229,781 kg). The overall vehicle length is 198 ft (60.35 m), the maximum LH2 tank diameter is 22.3 ft (6.8 m), and the total engine length (cylindrical body section) is 33.5 ft (10.2 m). The theoretical wing planform area is 2,550 $ft^2$ (237 $m^2$). The required mass ratio (MR) for ascent is 4.393 and the total ascent propellant mixture ratio (LOX/LH2) is 2.831. More detail on the vehicle geometry is available in reference 21.

Reference 13 discusses the concept of effective specific impulse, $I^*$, as a measure of the overall vehicle Isp taking into account ascent trajectory losses. For the RBCC SSTO, the effective specific impulse, $I^*$, is 512 sec as calculated by the rocket equation (equation 4). $\Delta V_t$ is the total inertial change in velocity from launch to orbit insertion (i.e. the ideal ΔV minus drag, thrust vector, and gravity losses). For the final design, the ideal ΔV is 32,893 ft/s (10,026 m/s) and the $\Delta V_t$ is 24,404 ft/s (7,438 m/s).

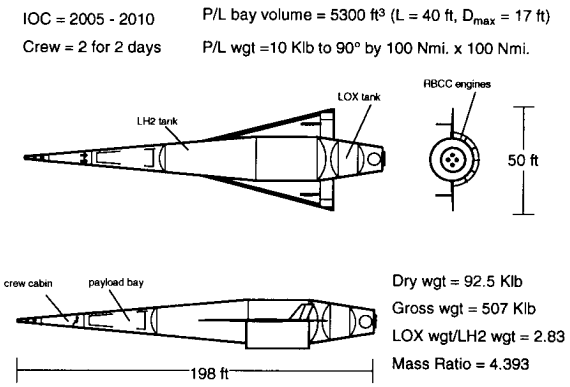


Figure 7 - Final RBCC SSTO Design

$$I^* = \frac{\Delta V_t}{g_c \ln(MR)} \qquad (4)$$

Figures 8a and 8b display the angle of attack (alpha), dynamic pressure, inertial velocity, and altitude history for the optimized ascent trajectory for the final vehicle design. An extremely simplified weight statement is listed in table 10. More detailed weight statement information is available in the appendices of reference 21.

For each point design in this study, new engine performance information (Isp and thrust) was generated based on current engine geometry (inlet height, capture area), vehicle geometry (forebody angle, body diameter), and ascent trajectory (airflow rates, velocities, altitudes). Graphs of cowl-to-tail Isp , equivalence ratio (ϕ), aerodynamic drag, and cowl-to-tail thrust vs. Mach number for the *final* RBCC SSTO design and trajectory are given in figures 9 and 10. Note that equivalence ratio was limited to linear interpolation between four reference point values. The values for ϕ at each of the four reference points were optimized by POST for each ascent trajectory. Other point design vehicles had different engine performance characteristics.

For the final vehicle, the engine weight, including cowl, is 23,338 lbs (10,586 kg). The sea-level static engine thrust-to-weight ratio is 26.04 in ejector mode. Without the cowl, the engine thrust-to-weight ratio is 40.9.

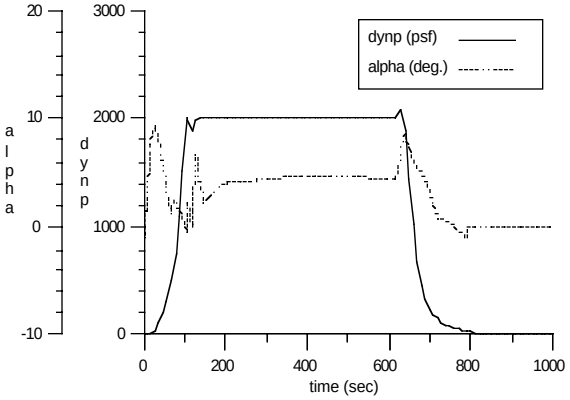


Figure 8a - Dynamic Pressure and alpha vs. Time for Final Design

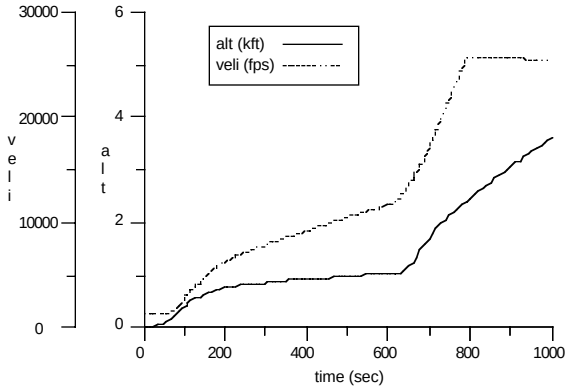


Figure 8b - Altitude and Inertial Velocity vs. Time for Final Design

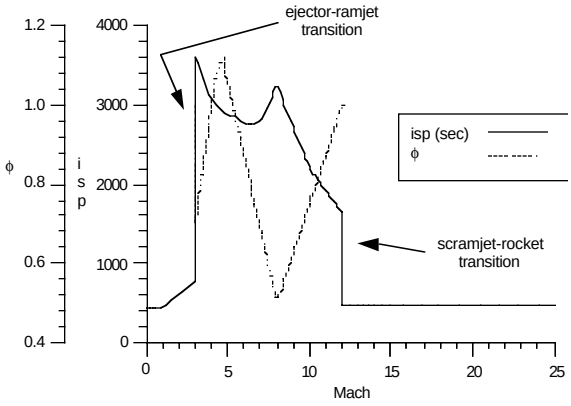


Figure 9 - Isp and ϕ vs. Mach for Final Design

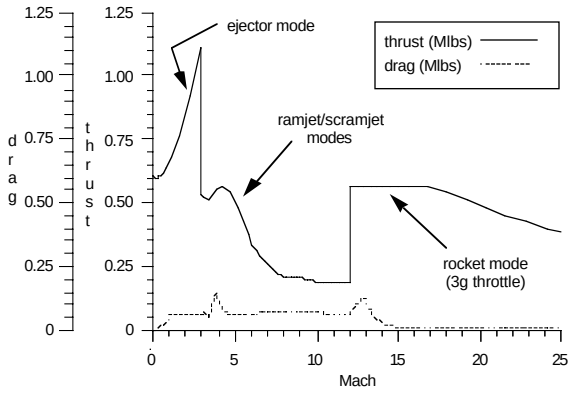


Figure 10 - Thrust and Drag vs. Mach for Final Design

Table 10 - Simplified Weight Statement

| Item | lbs | kg |
|---|---|---|
| Structures | 37,685 | 17,094 |
| TPS | 11,297 | 5,124 |
| Engine (no-cowl) | 17,809 | 8,078 |
| Other Weights | 16,457 | 7,465 |
| Margin (10%) | 9,250 | 4,196 |
| **Dry Weight** | **92,498** | **41,957** |
| Crew and Gear | 1,890 | 857 |
| Payload | 10,000 | 4,536 |
| Ascent Prop | 391,265 | 177,477 |
| Other Fluids | 10,922 | 4,954 |
| **Gross Weight** | **506,575** | **229,781** |

The passive components of the vehicle's thermal protection system are primarily determined by radiation equilibrium temperatures on various parts of the vehicle surface. For the final RBCC SSTO design, 33% of the total body area (excluding wings) was protected by advanced carbon-carbon and 34% by Inconel TPS. The remaining areas (including portions of the wings) were either actively cooled or left as titanium-aluminide "hot structure" as appropriate.

## ISSUES AND CONCERNS

The final vehicle design has been logically selected and care has been taken to account for all of the major effects in a very complex design space. However, there are a number of issues and concerns pertaining to analysis methods and tools that remain to be considered by future researchers. For various reasons (time, lack of detailed expertise, etc.), the

following issues received only cursory treatment in this research.

1) Lift-off Mode

Phase 1 of this research [11] indicated a clear weight advantage of vertical lift-off vs. horizontal lift-off. In some cases, horizontal lift-off vehicles were penalized as much as 25,000 lbs (11,340 kg) in terms of dry weight. The RBCC engine operates in a high thrust ejector mode at lift-off. It can lift-off vertically and take advantage of reduced wing weight and reduced landing gear requirements. However, since cowl wrap angle was optimized to 180°, there is a problem with asymmetric thrust at lift-off. A combination of RCS augmentation from the nose thrusters, engine thrust vectoring, and aerodynamic controls (with sufficient speed) will be required to ensure that the vehicle lifts-off smoothly and is able to make an early transition to nearly horizontal flight. The engines may have to be separated into 90° modules and placed at the sides of the vehicle in order to reduce asymmetric thrust. Additional work is needed in this area.

2) Reentry Trajectory

The RBCC SSTO is designed for a shuttle-like unpowered, lifting reentry from orbit. The winged cone configuration provides a relatively high lift-to-drag ratio (L/D = 1.7 at trimmed reentry conditions) so cross range capability and reentry loads were not considered issues. However, the position of the cowl (particularly the cowl lip) on the lower surface of the vehicle will present a heating problem. During ascent the cowl lip is actively cooled with hydrogen flowing to the engine. Reentry heating is not expected to be as severe as ascent heating, but may still require special active cooling provisions for some parts of the body.

3) Ascent Control and Trim

The ascent trajectory trim and aerodynamic control requirements were not simulated for this research. While angles of attack are relatively low, the lengthy acceleration time in the atmosphere could cause trim losses to become significant. Decreases in ramjet/scramjet performance at angles-of-attack were not taken into account. In addition, precise aerodynamic control and quick aerosurface reaction times will be required to maintain a constant dynamic pressure boundary during scramjet operation. Additional research is recommended in these areas to determine the overall impact on the vehicle design.

4) Landing Conditions

Phase 1 of this research [11] demonstrated the dry weight advantage of a vehicle designed using the RBCC engine *without* the supercharging fan. However, engine *with* the supercharging fan has advantages at landing that should be considered — powered go-around, loiter, self-ferry, etc. Decision makers should consider whether these advantages are worth the additional vehicle weight incurred. In addition, aerodynamic performance during landing should be examined with more detail analysis tools. The aerodynamic analysis tool used for this research is incapable of accurate prediction for conditions with the large degree of separated flow likely to exist for a cone at high angle of attack. Additional work could help refine landing speed and wing loading requirements.

5) Vehicle Geometry

The research was limited to the optimization of a few parameters of a *conical* configuration only. One of the primary advantages of a conical shape is a high engine capture area. However, since the cowl wrap angle was optimized to 180° (with indications that the true optimum could be even lower), the question is raised as to whether a conical configuration is the preferred geometry. There are structural advantages to the circular cross section propellant tank in a conical geometry, but the upper surface of the cone compresses air that is not fed into an engine resulting in increased drag. Alternate vehicle configurations (including those with 2-D inlet compression surfaces) should be considered to determine the advantages of one shape over another. If the shape is changed, most of the systems-level design variables will also have to be reconsidered. It is unreasonable to assume that optimized variables like $T/W_o$ and $M_{tr}$ are independent of vehicle shape. Multidisciplinary design optimization (MDO) tools such as those employed in the current research would be valuable in such a shape comparison study.

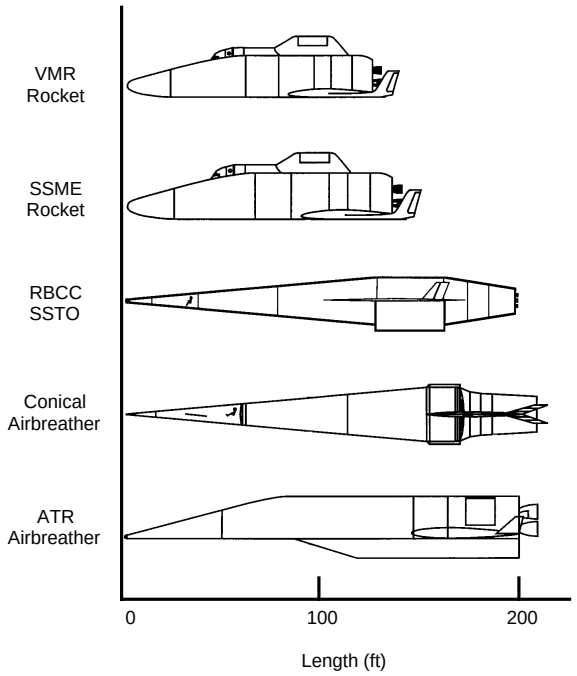


Figure 11 - SSTO Design Options

## VEHICLE COMPARISONS

In reference 30, Freeman compares several advanced launch vehicle design options. Four of the vehicles are advanced technology SSTO's — an SSME powered rocket, a rocket with a variable mixture ratio (VMR)/dual expansion nozzle engine, a multi-cycle SSTO combining air-turborocket (ATR) and rocket propulsion, and an advanced conical airbreather combining a turbo-based low speed cycle, ramjet, scramjet, and rocket modes. Wilhite [22] later updated and improved the structural MERs for the two rocket vehicles. The two airbreathing concepts are horizontal launch.

Freeman's vehicles are all designed to similar guidelines as the current RBCC SSTO (i.e. design for performance, advanced technologies, 10% dry weight margins, 10,000 lb (4,536 kg) payload to a 100 Nmi. (185 km) circular polar orbit, small crew sizes, and two day mission duration). Some of Freeman's concepts do employ slush hydrogen propellants. However, comparisons to the current vehicle are appropriate. These four concepts are shown with the current vehicle in figure 11.

The conical airbreather (conical AB) SSTO is very similar in geometry to the RBCC SSTO vehicle, but there are several distinct differences. The RBCC SSTO uses ejector mode operation for the initial stage of flight. The conical airbreather uses a turbo-based low speed cycle. The RBCC engine has a lower Isp in ejector mode than the turbo-based low speed cycle, but the RBCC engine is considerably lighter for a given thrust. In addition, the cowl wrap angle on the conical airbreather is 360° compared to 180° for the RBCC SSTO. But perhaps most significant is the airbreathing to rocket transition ($M_{tr}$) during ascent. The RBCC SSTO transitions at Mach 12 while the conical airbreather remains in scramjet mode to over Mach 20!

The gross weights and dry weights of the five design options are shown in table 11 and figures 12 and 13. Wilhite's updated structural MER's have been applied to both rocket vehicles. The updated VMR rocket was previously published in reference 22. The RBCC SSTO compares very favorably in terms of both dry weight and gross weight. It is neither the lightest dry weight (the VMR rocket is lighter) nor the lightest gross weight (the conical AB is lighter), but it is second in both cases. This result is consistent with the earlier hypothesis that a combined-cycle vehicle might lie between rockets and airbreathers (figure 1), but the RBCC SSTO results lie closer to the preferred extreme than expected.

Table 11 - Advanced SSTO Comparisons

| Concept | Dry Weight (klbs) | Gross Weight (klbs) | Body Length (ft) |
|---|---|---|---|
| VMR Rocket | 90 | 1,108 | 125 |
| SSME Rocket | 99 | 1,107 | 134 |
| **RBCC SSTO** | **92** | **507** | **198** |
| Conical AB | 157 | 451 | 220 |
| ATR SSTO | 214 | 1,087 | 210 |

Although airbreathing engines tend to have higher Isp's than rocket engines, the rocket engines have a significant advantage in terms of engine sea-level thrust-to-weight ratio as shown in figure 14. Airbreathing engines are heavier due to inlets, cowls, etc. Note, the $T/W_o$ for the ATR SSTO is for the air-turborocket at sea level. The vehicle also switches to

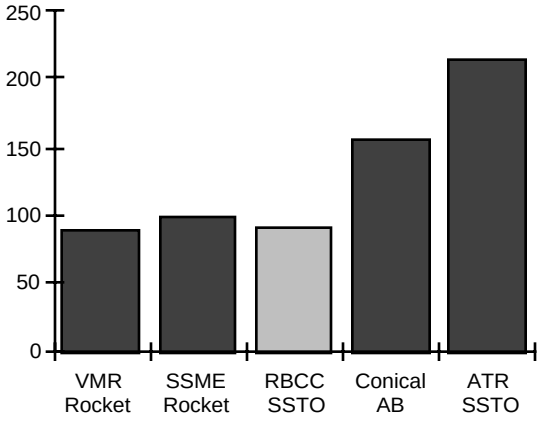


Figure 12 - Dry Weight (klbs) Comparison

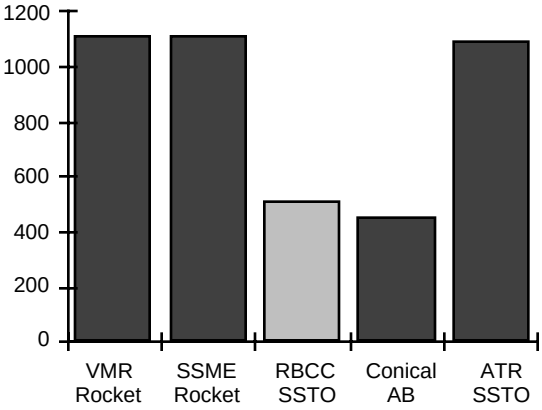


Figure 13 - Gross Weight (klbs) Comparison

an SSME-derived rocket engine at higher Mach numbers. The RBCC SSTO engine $T/W_o$ lies between the airbreathing and rocket extremes.

All of the values used for these comparisons are the results of conceptual, not detailed, design. The actual numbers are sure to change as the analysis is refined and some of the issues and concerns are resolved for all of the vehicles. In fact, all of the vehicles will need some adjustments to make them more "design for operations" oriented. However, the relatively favorable comparisons indicate that the RBCC SSTO is a very viable option for a next generation launch vehicle. The vehicle, and particularly the propulsion cycle, should continue to receive attention from advanced vehicle designers and decision makers.

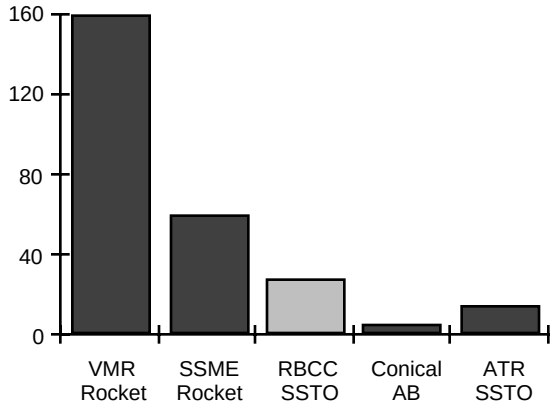


Figure 14 - Engine Installed $T/W_o$ Comparison

## CONCLUSIONS

A conical SSTO launch vehicle using rocket-based combined-cycle propulsion was successfully designed and optimized by using multidisciplinary design optimization tools. Three systems-level design variables were determined. Five design variables had been determined in an earlier phase of this study. A second-order response surface was created to approximate the changes in dry weight as the design variables are changed. The second-order model enables designers to quickly answer "what-if" questions about design changes.

Perhaps the most important conclusion is that the cowl wrap angle should be 180° (or less) rather than 360° as favored by previous researchers. The cowl wrap angle has the most significant effect on overall vehicle dry weight of all the variables considered. A larger cowl wrap angle produces a larger capture area and a higher thrust. These effects combine to produce a lower vehicle mass ratio, but this advantage is far outweighed by the increase in engine and cowl weight so that the resulting overall vehicle dry weight increase. Therefore, the lower cowl wrap angle (and lower engine weight) is preferred. This conclusion is highly dependent on the thrust-to-weight ratio of the airbreathing engine components.

Using Taguchi's method of robust design, it was determined that a scramjet-to-rocket mode transition Mach number of 12 will produce a vehicle that is less sensitive to unpredicted changes high speed

engine performance, engine weight, and body weight. While a $M_{tr}$ of close to 15 provides a slightly better dry weight, the advantages of robustness were considered more significant. Vehicles with higher $M_{tr}$'s use a relatively higher percentage of LH2 fuel and tend to have lighter gross weights and lower MR's. In this case the advantage is reflected in lower dry weights. However, this conclusion is highly dependent on ramjet/scramjet engine Isp (hence the argument for robust design). Significant degradations of engine Isp could quickly erode the advantages of higher transition Mach numbers. Therefore, the more robust $M_{tr}$ of 12 was selected for the final vehicle design in this study.

Throughout the design process, the initial vehicle lift-off $T/W_o$ was shown to be one of the least significant effects on dry weight and S/N. Higher lift-off $T/W_o$ vehicles have lower gravity losses, accelerate faster to Mach 3, and therefore have more time in airbreathing modes. The advantages translate to a lower MR. However, these advantages are almost exactly canceled by the increase in ejector component engine weight.

When compared to other advanced launch vehicle concepts, the RBCC SSTO proved to be very competitive. Advocates for combined-cycle propulsion argue that there is a potential to combine the best characteristics of rocket and airbreathing propulsion. This was largely proven to be true. The RBCC SSTO has a dry weight comparable to a rocket and a gross weight comparable to an airbreathing vehicle.

The MDO tools used (robust design and second-order response surface methods) were very important to the success of this research. Old fashioned "one-variable-at-a-time" trade studies would have been inadequate in the multivariable, complex design space of this vehicle. The growing field of MDO should continue to receive support and encouragement.

## RECOMMENDATIONS

In addition to the resolution of the issues and concerns mentioned in a previous section, there are several areas where additional research is recommended. These areas are related specifically to the conical RBCC design and the efforts to determine the optimum variable settings and to characterize the vehicle design space.

1) Extend the variable range for cowl wrap angle to values below 180°. Indications are that the true optimum lies below 180° and that significant weight savings could be obtained. Additional experimental point designs will be required to ensure that the optimum is interpolated (rather than extrapolated) from known point designs.

2) Include additional noise variables in the robust design technique. The method was very successful at locating a robust design point. Additional noise variables could include payload weight growth, dry weight margin growth, and boundary layer transition criteria (for heating).

## ACKNOWLEDGMENTS

This work was supported by cooperative agreement number NCC1-168 between North Carolina State University and NASA-Langley Research Center and by NASA Grant NAGW-1331 to the Mars Mission Research Center at North Carolina State University. The author also appreciates the support and assistance of Dr. Bill Escher at NASA-HQ, Dick Foster at Astronautics Corporation, Dr. Gerald Walberg at NCSU, Dr. Resit Unal at Old Dominion University, Dr. Alan Wilhite at NASA-LaRC, and members of the Vehicle Analysis Branch at NASA-LaRC including Doug Stanley, Roger Lepsch, Dick Powell, Walt Engelund, Ian "Mac" MacConochie, Larry Rowell, and Kay Wurster.

## REFERENCES

1. Wilhite, A. W., et. al., "Concepts Leading to the National Aero-Space Plane Program." AIAA paper 90-0294, January 1990.

2. Hunt, J. L., and J. Martin, "Aero-space Plane Figures of Merit." presented at the 4th International Aerospace Planes Conference, December 1992.

3. Stanley, D. O., et. al., “Rocket-Powered Single-Stage Vehicle Configuration Selection and Design.” AIAA paper 93-1053, February 1993.

4. Lepsch, R. A., D. Stanley, and R. Unal. “Application of Dual-Fuel Propulsion to a Single Stage AMLS Vehicle.” AIAA paper 93-2275, June 1993.

5. Copper, J. A., et. al. “Future single stage rockets: Reusable and reliable.” *Aerospace America*. February 1994.

6. Lerner, P. “Single Stage to...Where?” *Air & Space*. February/March 1994.

7. Escher, W. J. D., “Combined-Cycle and Hypersonic Propulsion - A Renewed Rocketdyne Initiative.” *Threshold* - Rocketdyne’s internal engineering journal of power technology, Issue No. 3, Summer 1988.

8. Escher, W. J. D. “Highlights of NASA’s Special ETO Program Planning Workshop on Rocket-Based Combined-Cycle (RBCC) Propulsion System Technologies.” AIAA paper 92-3811, July 1992.

9. Escher, W. J. D., and P. Czysz. “Rocket-Based Combined-Cycle Powered Spaceliner Concept.” IAF paper 93-S.4.478, October 1993.

10. Foster, R. W. “Optimization of the Rocket Mode Trajectory in a Rocket Based Combined Cycle (RBCC) Engine Powered SSTO Vehicle.” AIAA paper 89-2295, July 1989.

11. Olds, J. R., and G. Walberg. “Multidisciplinary Design of a Rocket-Based Combined Cycle SSTO Launch Vehicle using Taguchi Methods.” AIAA paper 93-1096, February 1993.

12. Phillips, W. P., et. al.. “Experimental Investigation of the Aerodynamic Characteristics for a Winged-Cone Concept.” AIAA paper 87-2484, August 1987.

13. Foster, R. W., W. Escher, and J. Robinson. “Studies of an Extensively Axisymmetric Rocket Based Combined Cycle (RBCC) Engine Powered SSTO Vehicle.” AIAA paper 89-2294, July 1989.

14. Foster, R. W., W. Escher, and J. Robinson. “Air Augmented Rocket Propulsion Concepts.” USAF Astronautics Laboratory Report AFAL-TR-88-004, April 1988.

15. MacConochie, I. O., R. Davis, and W. Freeman. “Filament Wound Metal Lined Propellant Tanks for Future Earth-to-Orbit Transports.” NASA TM-100594, October 1988.

16. Shaughnessy, J. D., et. al. “Hypersonic Vehicle Simulation Model.” NASA TM-102610, November 1990.

17 Anon. “A Study of Composite Propulsion Systems for Advanced Launch Vehicle Applications.” NASA contract NAS7-377, September 1966.

18. Brauer, G. L., et. al. “Program to Optimize Simulated Trajectories (POST).” NASA contract NAS1-18147, September 1989.

19. Sova, G. and P. Divan. “Aerodynamic Preliminary Analysis System II Part II - User’s Manual. NASA CR 182077, April 1991.

20. Engel, C. D., and C. Schmitz. “Miniver Upgrade for the AVID System.” NASA CR-172213, August 1983.

21. Olds, J. R. “Multidisciplinary Design Techniques Applied to Conceptual Aerospace Vehicle Design.” PhD Dissertation. North Carolina State University, July 1993.

22. Wilhite, A. W., et. al. “Advanced Technologies for Rocket Single-Stage-to-Orbit Vehicles.” AIAA paper 91-0540, January 1991.

23. Phadke, Madhav. Quality Engineering Using Robust Design. NJ : Prentice-Hall, 1989.

24. Taguchi, G, and S. Konishi. Orthogonal Arrays and Linear Graphs. American Supplier Institute, 1987.

25. Taguchi, G., E. Elsayed, T. Hsiang. Quality Engineering in Production Systems. NY:McGraw-Hill, 1989.

26. Olds, J. R. “The Suitability of Selected Multidisciplinary Design Techniques to Conceptual Aerospace Vehicle Design.” AIAA paper 92-4791, September 1992.

27. Stanley, D., R. Unal., and R. Joyner “Application of Taguchi Methods to Dual Mixture Ratio Propulsion System Optimization for SSTO Vehicles.” AIAA paper 92-0213, January 1992.

28. Bush, L., and R. Unal. “Preliminary Structural Design of a Lunar Transfer Vehicle Aerobrake.” AIAA paper 92-1108, February 1992.

29. Montgomery, D. Design and Analysis of Experiments. NY: John Wiley and Sons, 1991.

30. Freeman, D. C., et. al. “Design Options for Advanced Manned Launch Systems (AMLS).” AIAA paper 90-3816, September 1990.